# An adaptive coupled level set and moment-of-fluid method for simulating droplet impact and solidification on solid surfaces with application to aircraft icing

Mehdi Vahab*, Chaoxu Pei†, M. Yousuff Hussaini‡ and Mark Sussman§
*Florida State University, Tallahassee, FL 32306*
Yongsheng Lian¶
*University of Louisville, Louisville, KY 40292*

**An adaptive multiphase hybrid level set moment-of-fluid method is developed to study the impact and solidification of water droplets on flat surfaces. The numerical simulations are validated by comparison to analytical results and experimental observations. The present simulations demonstrate the ability of the method to capture sharp solidification front, and handle contact line dynamics, and the simultaneous impact, merging and freezing of a drop. Parameter studies have been conducted, which show the influence of the Stefan number on the regularity of the shape of frozen droplets. Also, it is shown that impacting droplets with different sizes create ice shapes which are uniform near the impact point and become dissimilar away from it. In addition, surface wettability determines whether droplets freeze upon impact or bounce away.**

## Nomenclature

| | |
|---|---|
| $Bo$ | Bond number |
| $C_p$ | Heat capacity, erg/(gm K) |
| $D$ | Deformation tensor, 1/s |
| $F$ | Volume fraction |
| $\mathbf{g}$ | Gravitational acceleration, cm/s$^2$ |
| $H$ | Heaviside function |
| $k$ | Thermal conductivity, erg/(s cm K) |
| $L$ | Latent heat of fusion, erg/gm |
| $M$ | Number of phases |
| $n$ | Unit normal vector |
| $p$ | Pressure, g/(cm s$^2$) |
| $Pr$ | Prandtl number |
| $M$ | Number of phases |
| $St$ | Stefan number |
| $T$ | Temperature, $K$ |
| $\mathbf{u}$ | Velocity, cm/s |
| $V_n$ | Freezing rate, cm/s |
| $We$ | Weber number |
| $\kappa$ | Curvature, 1/cm |
| $\mu$ | Viscosity, g/(cm s) |
| $\phi$ | Level set function, cm |

*Post Doctoral Research Associate, Department of Mathematics
†Graduate Student, Department of Mathematics
‡Sir James Lighthill Professor of Mathematics and Computational Science & Engineering
§Professor, Department of Mathematics
¶Associate Professor, Mechanical Engineering

$\rho$ Density, g/cm$^3$
$\sigma$ Surface tension, g/s$^2$

*Subscript*
$b$ Substrate
$c$ Cold
$h$ Hot
$f$ Freezing
$g$ Gas, air
$l$ Liquid, water
$m$ Phase number
$p$ Supercooled
$s$ Solid, ice

# I. Introduction

One of the main causes of aircraft icing is the impact and solidification of supercooled liquid water droplets on aircraft surfaces during flight. Ice formation can appear on the edges of a wing or a propeller, changing the aerodynamic features of the aircraft. Ice formation leads to reduction of thrust or lift, increased drag and angle of attack, and added weight, all of which increase accident risk and fuel consumption.[1] Therefore, numerous programs and studies have been developed to address the aircraft icing problem,[2–4] and the Federal Aviation Administration (FAA) has imposed regulations regarding the performance of aircraft in icing conditions.

Various experimental studies have been performed to examine the ice formation problem. These studies document the shape of ice formation on different types of aircraft wings. Environmental conditions such as temperature, wind speed, water content and/or droplet size have been varied and then aerodynamic performance parameters for ice-accumulated wings have been measured. We remark that the experimental results reported by Shin and Bond[5] for ice formation at temperatures as low as -15 °F are repeatable compared to experiments conducted near freezing temperatures. This is a motivating factor for our work, because a numerical simulation is more repeatable through out the range of possible supercooled temperatures of interest.

The Addy[6] experiments concluded that exposure to atmospheric icing conditions described by FAA FAR Appendix 25 C has notable effects on lift coefficient and stall angle. However, the sensitivity of aerodynamic properties of the wing to the Reynolds number is significantly reduced when the leading edge is covered by ice. Other recent experiments[7] categorized ice formation based on the observed aerodynamics into four types (roughness, streamwise, spanwise ridge, and horn) and measured the changes in the aerodynamic features such as lift, drag and moment coefficients. The horn shape has the most adverse effect. Also, Bragg et al.[7] reported that the least significant ice formation, roughness shape, measurably changes the aerodynamic properties of the airfoil. This follows the previous results[6] that surface texture and irregularities of the aircraft icing are important in the study of aircraft icing.

Numerical simulations of aircraft icing have been conducted in order to assist the aircraft design and certification process. Some examples of numerical simulation tools used to assist practitioners are LEWICE,[8,9] CANICE,[10,11] and FENSAP-ICE.[12] These codes often represent droplets with particles for predicting the accumulation of ice on aircraft parts. The particle approximation is appropriate for small droplets. For larger droplets, the dynamics of droplet trajectory, impact, and solidification are more complex.[13] Before impact, a single droplet might deform or oscillate because of its surrounding environment. Upon impact, a droplet may bounce, spread or splash. Also, freezing may not be instantaneous upon droplet impact, which might then lead to the creation of run-back streams or satellite droplets which freeze further downstream.

Aircraft icing conditions are more severe when *supercooled large droplets* (SLD) are present.[14] Some airplane accidents caused by icing were in flying conditions in which the SLD regime was present.[15] Generally, SLD are larger than 50 $\mu$m in diameter and they are formed in different ways. For example, falling snow may melt as it passes through a warm layer of air thereby making large droplets which continue to fall through a lower cold layer of air. These droplets do not freeze again until they impact an object. Another mechanism for the creation of SLD is that smaller cloud droplets falling at different speeds may collide and merge to form larger droplets.[1] The impact and solidification dynamics involving SLD are more complex

than that involving cloud-size droplets. SLD may splash after impact and create smaller droplets which in turn merge, freeze, hit the surface, or shed away. Splashing models that take into account the presence of droplets in the SLD regime have been developed for inclusion in numerical ice accretion codes.[16] However, these models do not capture the intricate details associated with SLD impact, merging, splitting, generation of downstream flow, and solidification.[17,18] Finally, we note that it has been reported that splashing of large droplets depends on the ambient pressure which varies with flight conditions.[19,20]

The modeling and simulation of a multiphase system that has phase change (e.g. freezing/melting or vaporization/condensation) is a complex task.[21,22] Since the scale of the phase transition region is much smaller than the problem domain size, we assume the interface separating phases is perfectly sharp.[23] In our simulations, we prescribe that the phase change is a constant temperature process, the latent heat is released/absorbed over an infinitely thin region, and that volume expansion takes place only at the interface where phase change is taking place. A common sharp-interface numerical approach is the volume-of-fluid (VOF) method for representing the deforming interface at which phase change is taking place. Pasandideh-Fard et al.[24] implemented the VOF method in order to simulate the impact and solidification of molten tin droplets on a stainless steel plate and developed a model for the maximum spread diameter. Later they developed another volume-tracking approach in order to simulate the impact and solidification of droplets on an oblique surface.[25] Le Bot et al. [26] constructed the VOF method in order to simulate the concurrent impact and solidification of indium droplets on a cold surface. Le Bot et al. [26] applied their method for studying coating and thin film manufacturing processes. Finally, a VOF method was developed in order to simulate the solidification of a hydrogen droplet in cryogenic helium, which involves the vaporization of helium.[27,28]

Besides the VOF method for simulating phase change with a sharp interface, alternative approaches are the level set method and the front-tracking method. Example level set implementations are the work of Zheng and Zhang[29] (adaptive level set method for droplet spreading and solidification), Mihalef et. al.[30] (coupled level set and VOF method for simulating boiling), and Gibou et. al.[31] (ghost fluid approach for incompressible multiphase flows with boiling). Example front-tracking implementations are the work of Esmaeeli and Tryggvason[32,33] (front-tracking method for film boiling) and Vu et al.[34] (front-tracking for solidification of droplets on a flat surface while considering the volume change due to solidification).

The moment-of-fluid method (MOF)[35–41] is a generalization of the VOF method. In addition to the volume fraction of each fluid in a computational cell, the centroid of each material in the cell is also considered. This information is used to reconstruct the interface. Lian et. al.[42] have recently used a MOF method to study the impact of SLD on a dry surface. They showed that an adaptive MOF method can accurately capture the interface in splashing conditions. A coupled level set MOF method would be advantageous for simulating droplet impact and solidification. The level set representation allows for sharp treatment of interfaces undergoing phase change because the normal vector, curvature, and expansion source term are readily available from the level set function. At the same time, the volume fraction and moment information allow one to reconstruct sharp volume preserving multimaterial interfaces.

Treatment of the triple point, whereat the three phases -gas, liquid, and solid - of the system coexist in thermodynamic equilibrium, is a key issue that needs attention when simulating a multiphase system with more than two materials. Gibou et. al.[31] did not consider the triple point case. Son and Hur[43] studied the triple point dynamics for the flat solid surface. Pasandideh-Fard et al.[25] only set the liquid-solid contact angle based on the estimation of normal vectors from the VOF representation. Le Bot et al.[26] simply employed a static contact angle between the substrate and the liquid part of the droplet. Bonhomme et. al.[44] resolved the triple point dynamics in their work using a VOF method. Here, we use the level set functions derived from the MOF reconstruction near triple points in order to evaluate the normal vectors and curvatures accurately and capture the triple point dynamics; all interfacial tension forces are considered.

The goal of the current study is to do numerical simulations for the impact and solidification of supercooled water droplets with aeronautics applications in mind. An adaptive multiphase moment of fluid method, capable of capturing sharp solidification fronts, is employed to simulate the multiphase system for this problem. Several numerical tests are performed and comparison with analytical solutions and experimental results are done in order to validate the numerical method. Also, parameter studies regarding droplet size, Stefan number and surface wettability are done for the droplet impact and solidification problem.

## II. Physical and Mathematical Model

The real-world problem consists of the impact and solidification of (supercooled) water droplets on an airplane part, such as a wing. In this study, we limit our scope to the impinging of a single droplet on a surface (Figure 1.a). For the sake of simplicity, parameter study is done for the normal impact and solidification of a spherical droplet on a flat surface (Figure 1.b).

The physical system is modeled by considering the conservation of mass, momentum and energy for immiscible fluids along with the phase change dynamics of the freezing process and surface tension dynamics on material interfaces and at triple points. In this model, we do not consider the freezing nucleation process by making the assumption of a preexisting thin layer of ice where the freezing process is likely to start. Also, the effects of evaporation or formation of the condensation halo, formation of the mushy zone, and the Marangoni phenomenon are ignored.

We assume the physical properties of the materials are known. An initial impact velocity is imposed on the droplet. Surrounding air velocity is set according to the incompressible continuity condition. Also, we assume no cross-flow in this study. The outflow boundary condition is applied on the open boundaries along with the no-slip wall condition for the bottom part of the domain. For the temperature, initial values for the droplet and ambient temperatures are set based on the corresponding experiments in each case, and the bottom part of the domain is kept at a prescribed temperature.

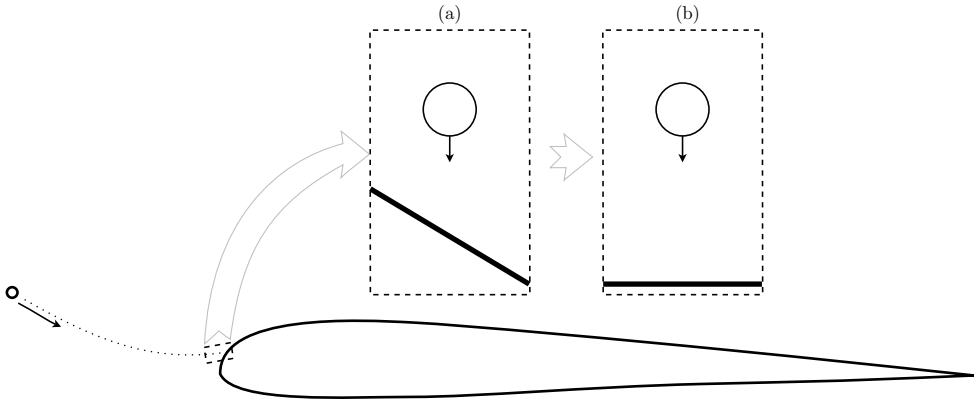


**Figure 1. Schematic model of the physical problem. (inset) (a) Computational domain. (b) Simplified domain for the analysis in this study.**

A mathematical model of the physical system described above is as follows. The flow of a multiphase system consisting of $M$ phases is governed by the incompressible Navier-Stokes equations of immiscible flows with the following one-fluid formulation for conservation of mass, momentum and energy:

$$\nabla \cdot \mathbf{u} = 0, \tag{1}$$

$$\frac{\partial \rho \mathbf{u}}{\partial t} + \nabla \cdot (\rho \mathbf{u} \otimes \mathbf{u}) = -\nabla p + \nabla \cdot (2\mu D) + \rho \mathbf{g} - \sum_{m=1}^{M} \gamma_m \kappa_m \nabla H(\phi_m), \tag{2}$$

$$\frac{\partial}{\partial t}(\rho C_p T) + \nabla \cdot (\rho C_p T \mathbf{u}) = \nabla \cdot (k \nabla T), \tag{3}$$

where vector $\mathbf{u} = (u, v, w)$ is the velocity vector, $t$ is the time, $\mathbf{g}$ is the gravitational acceleration vector, $D$ is the rate of deformation tensor,

$$D = \frac{\nabla \mathbf{u} + (\nabla \mathbf{u})^T}{2} \tag{4}$$

and $\rho$, $p$ and $\mu$ are the combined density, pressure and viscosity respectively for material $m$. A combined quantity $y$ is defined as follows,

$$y \equiv \sum_{m=1}^{M} y_m H(\phi_m), \tag{5}$$

where $y_m$ is the quantity defined for material $m$, and $H$ is the Heaviside function defined as

$$H(\phi) = \begin{cases} 1 & \phi \geq 0 \\ 0 & \text{otherwise} \end{cases}. \tag{6}$$

The level set function $\phi_m$ is defined for material $m$ and satisfies,

$$\phi_m(\mathbf{x},t) = \begin{cases} > 0 & \mathbf{x} \in \text{material } m \\ \leq 0 & \text{otherwise} \end{cases}. \tag{7}$$

In the energy equation (3), $T$ is temperature, $C_p$ is the heat capacity and $k$ is thermal conductivity.

The jump condition on the material interface is satisfied by the last term in (2), where $\kappa_m$ is the curvature,

$$\kappa_m = \nabla \cdot \frac{\nabla \phi_m}{|\nabla \phi_m|}, \tag{8}$$

and $\gamma_m$ is defined based on the surface tension coefficients, $\sigma_{m_1 m_2}$. For $M = 3$ they are defined as,

$$\gamma_1 = \frac{\sigma_{12} + \sigma_{13} - \sigma_{23}}{2}, \tag{9}$$

$$\gamma_2 = \frac{\sigma_{12} + \sigma_{23} - \sigma_{13}}{2}, \tag{10}$$

$$\gamma_3 = \frac{\sigma_{13} + \sigma_{23} - \sigma_{12}}{2}. \tag{11}$$

The domain of each material is governed by the level set equation,

$$\frac{\partial \phi_m}{\partial t} + \mathbf{u}.\nabla \phi_m = 0,\ m = 1, \ldots, M. \tag{12}$$

The continuity equation (1) is enforced in the whole domain, except at the solidification front where the following jump condition is applied:

$$[\mathbf{u} \cdot \mathbf{n}] = -\left[\frac{1}{\rho}\right] V_n\, \rho_l, \tag{13}$$

where $V_n$ is the freezing rate in the front normal direction and $[x] \equiv x_s - x_l$. Subscripts $s$ and $l$ indicate variables related to *solid* and *liquid* phases respectively. The normal vector $\mathbf{n}_m$ is defined as,

$$\mathbf{n}_m = \frac{\nabla \phi_m}{|\nabla \phi_m|}. \tag{14}$$

The normal vector at the freezing front, $\mathbf{n}$, is defined to point from ice to liquid. The freezing front has the constant temperature

$$T = T_{\mathrm{f}}, \tag{15}$$

with the freezing rate

$$V_n = \frac{[k \nabla T] \cdot n}{L \rho_l}, \tag{16}$$

where $L$ is the latent heat of fusion.

Initially, temperature is known for all the materials. The droplet velocity is set to the impact velocity. A pre-processing projection step is done to make the whole velocity field divergence-free, enforcing continuity equation (1), thus setting the air velocity field accordingly. The material level set functions are initialized by the problem configuration. On the bottom boundary, a no-slip wall condition is applied and temperature is kept at the initial value. On the outflow boundaries, velocity is extrapolated and temperature is kept at the ambient value.

## III. Numerical Method

The numerical method used in this study is based on the adaptive multiphase method of Li et al.[45] We use a moment-of-fluid reconstruction in the cells with 3 or more materials. For cells with two materials, a CLSVOF reconstruction is applied.

To solve the governing equations described in Section II, we proceed as follows:

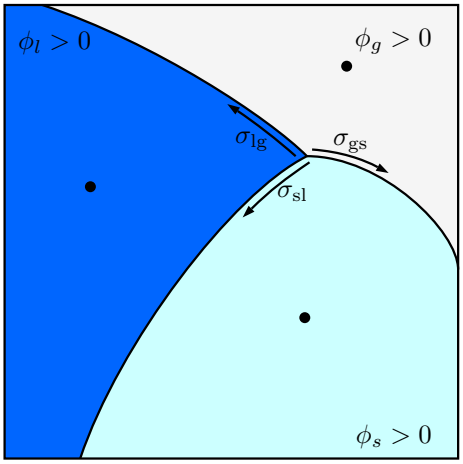


**Figure 2. A cell containing a triple point. Each dot shows the position of the moment for the corresponding phase. Moment of fluid reconstruction is used in this cell.**

- **Advection:** We solve the advection parts of (2) and (3) and we also advect the interface quantities $F_m$ (volume fraction), $\mathbf{x}_m$ (centroids), and $\phi_m$ (12) (level set functions). After interface advection, the level set functions are replaced with the exact signed distance to the coupled level set and moment-of-fluid piecewise linear reconstructed interface as well as closest point information $\mathbf{x}_{\text{closest}}$ is derived (see (Figure 3)).

- **Stefan Problem:** The freezing rate is evaluated from (16). For any point $\mathbf{x}$ in the vicinity of the interface, the closest point on the liquid-ice interface, $\mathbf{x}_{\text{closest}}$, is found. A point with distance $\Delta x$ in the front normal direction, $\mathbf{x}_{\text{interpolation}}$, is located in the liquid (ice), and the temperature $T(\mathbf{x}_{\text{interpolation}})$ is evaluated using a limited least squares procedure using only neighbor liquid (ice) cell temperature values. $T(\mathbf{x}_{\text{interpolation}})$ and $T(\mathbf{x}_{\text{closest}}) = T_f$ are used to evaluate the freezing rate in the front normal direction (Figure 3). Then, the level set values are updated, taking into account the freezing rate of the solidification front:

$$\frac{\partial \phi_s}{\partial t} - V_n |\nabla \phi_s| = 0, \tag{17}$$

$$\frac{\partial \phi_l}{\partial t} + V_n |\nabla \phi_l| = 0. \tag{18}$$

  The volume fractions are also adjusted in order to take into account the conversion of water to ice:

$$F_s := F_s^{\text{old}} + F(\phi_s^{\text{new}}) - F(\phi_s^{\text{old}}). \tag{19}$$

- **Temperature and Viscous Diffusion:** The energy equation (3) is solved using the backwards Euler method. The saturation temperature boundary condition is discretized using the second order method of Gibou et. al.[46] An explicit sub-cycling method from Li et al.[45] is used to solve the viscous diffusion part of (2).

- **Pressure Projection:** The remaining parts of (2) are solved using a projection method,[45]

$$\mathbf{u}^{n+1} = \mathbf{u}^* - \Delta t \frac{\nabla p}{\rho}, \tag{20}$$

$$\nabla \cdot \frac{\nabla p}{\rho} = \frac{1}{\Delta t} \left( \nabla \cdot \mathbf{u}^* - \frac{\mathrm{d}H}{\mathrm{d}\phi} |\nabla \phi| \left[ \frac{1}{\rho} \right] V_n \rho_l \right). \tag{21}$$

To keep the ice phase from moving, the velocity at all *ice faces* are set to zero. An ice face is a cell face in which neither adjoining cell is water but at least one is ice.

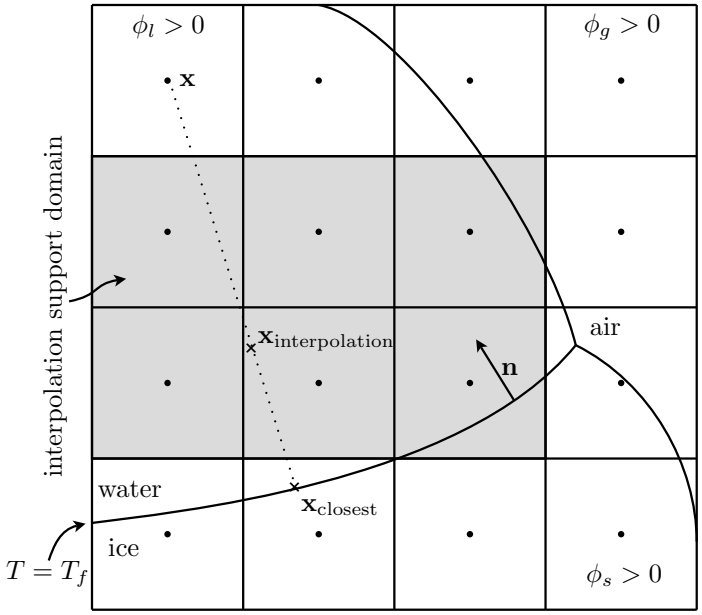


**Figure 3. Evaluation of the freezing rate $V_n$. Unit normal vector on liquid-ice front is defined $\mathbf{n} = -\nabla\phi_s/|\nabla\phi_s|$.**

## IV. Numerical Simulations and discussion

The following dimensionless parameters are considered to analyze the problems:

- Dimensionless position: $\mathbf{x}^* = \mathbf{x}/r_c$, where the characteristic length $r_c$ is the radius for a spherical droplet, or the wetting radius for a droplet on a surface.
- Dimensionless time: $t^* = t/t_c$ where $t_c = \rho_l C_{pl} r_c^2/k_l$.
- Dimensionless speed: $\mathbf{u}^* = \mathbf{u}/u_c$ where $u_c = r_c/t_c$.
- Dimensionless temperature: $T^* = (T - T_c)/\Delta T$, where $\Delta T = T_h - T_c$
- Stefan number: $St = C_{pl}\Delta T/L$
- Prandtl number: $Pr = C_{pl}\mu_l/k_l$.
- Bond number: $Bo = \rho_l g r_c^2/\sigma$.
- Weber number: $We = \rho_l u_c^2 r_c/\sigma$.
- Density ratios: $\rho_{sl} = \rho_s/\rho_l$, $\rho_{gl} = \rho_g/\rho_l$ and $\rho_{bl} = \rho_b/\rho_l$
- Viscosity ratios: $\mu_{sl} = \mu_s/\mu_l$, $\mu_{gl} = \mu_g/\mu_l$ and $\mu_{bl} = \mu_b/\mu_l$.
- Heat capacity ratios: $C_{psl} = C_{ps}/C_{pl}$, $C_{pgl} = C_{pg}/C_{pl}$ and $C_{pbl} = C_{pb}/C_{pl}$.
- Thermal conductivity ratios: $k_{sl} = k_s/k_l$, $k_{gl} = k_g/k_l$ and $k_{bl} = k_b/k_l$.
- Surface tension ratios: $\sigma_{ls,gl} = \sigma_{ls}/\sigma_{gl}$, $\sigma_{lb,gl} = \sigma_{lb}/\sigma_{gl}$, $\sigma_{sb,gl} = \sigma_{sb}/\sigma_{gl}$ , $\sigma_{gs,gl} = \sigma_{gs}/\sigma_{gl}$and $\sigma_{gb,gl} = \sigma_{gb}/\sigma_{gl}$.

Here we note that the numerical outflow boundary condition is imposed by extrapolating the velocity field and setting a constant pressure value at the corresponding boundaries. Also the temperature at a outflow boundary is set to the infinity/air temperature based on the test case.

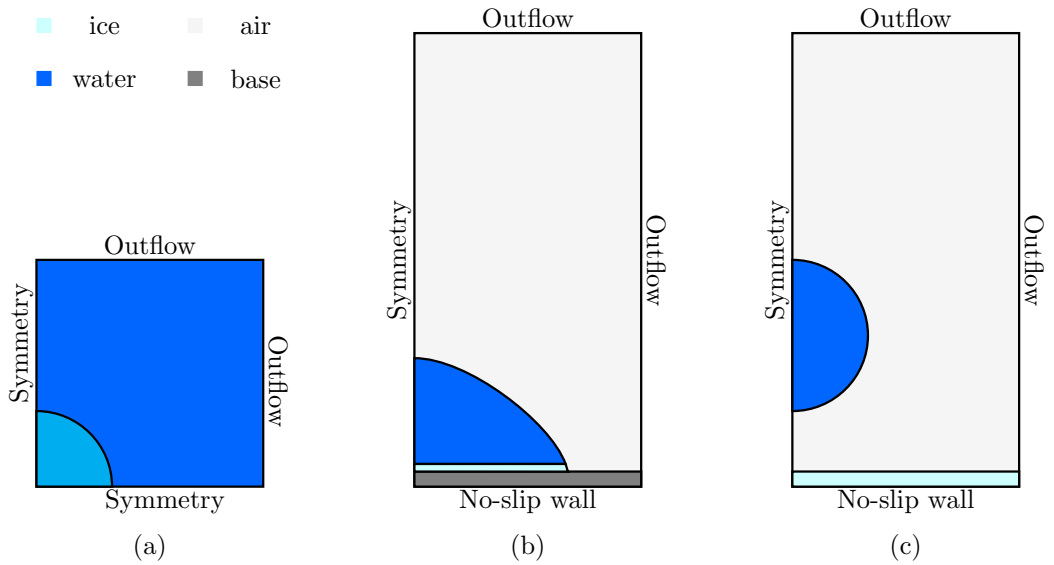


**Figure 4. Numerical domains and initial/boundary conditions for (a) radial growth of freezing circular front, (b) solidification of a water droplet at rest on a flat surface, and (c) impact and solidification of a water droplet on a flat surface**

### IV.A. Radial growth of freezing circular front

The radial growth of a freezing front of a circular ice phase surrounded by supercooled liquid is considered. Radius of the freezing front is $R$. The ice phase, $r \leq R$, is at freezing temperature $T_f$, and the liquid phase, $r > R$, is at temperature $T_p < T_f$ initially, that is $T_l(r) = T_p$ as $r \to \infty$ (see Figure 4.a for the initial and boundary conditions). Carslaw and Jaeger[47] derived the analytical solution for this problem. The radius of the freezing front $R$ is given by

$$R = 2\lambda\sqrt{k_l t}, \tag{22}$$

where $\lambda$ is the root of

$$\lambda^2 \exp(\lambda^2)\,\mathrm{Ei}(-\lambda^2) + St = 0, \tag{23}$$

where $\mathrm{Ei}(x)$ is the exponential integral function.

A $2\times2$ computational domain (dimensionless units) with $64\times64$ base grid and 2 or 3 levels of AMR is used for simulation of this problem. The initial ice phase is a disk with radius 0.05 (dimensionless units) at the center of the domain. The temperature in the liquid is initialized with the exact temperature corresponding to $R = 0.05$. Other dimensionless parameters are $St = 1/4$, $1/8$ or $1/16$, $Pr = 7.25$, $Bo = 0$, $We = \infty$, $\rho_{sl} = 1$, $C_{psl} = 1$ and $k_{sl} = 0$. The radius of the ice disk grows with $\sqrt{t}$ in time. Increasing Stefan number makes $\lambda$ larger and implies that freezing front is expanding faster. Figure 5.a shows the interface position in time from the simulation and exact solution for two values of Stefan number. The interface position converges under AMR grid refinement with order 1.58 under L-1 norm (see Figure 5.b).

### IV.B. Solidification of a water droplet at rest on a flat surface

For this test, we simulate the solidification of a water droplet on a flat substrate. Experiments for this problem are reported in Enríquez et al.[48] The droplet temperature is initially at the freezing level: $T = T_f = 273.15\,\mathrm{K}$. We introduce an ice layer with the temperature $T = T_p = 253.15\,\mathrm{K}$ at the contact surface of the droplet and substrate. The thickness of the initial seed ice layer is 0.05 (dimensionless units). The substrate is also initially supercooled at $T = T_p = 253.15\,\mathrm{K} < T_f$ (see Figure 4.b for the initial and boundary conditions). Simulations show the vertical advance of the freezing front. The computational domain is an RZ 3D axisymmetric domain with size $1.25 \times 2.5$ (dimensionless units). A $32 \times 64$ base grid with 1 level of adaptivity is used. The dimensionless parameters for this problem are: $St = 0.25$, $Pr = 14.4$, $Bo = 0.54$, $We = 1.4e-7$ $\rho_{gl} = 0.001$, $\rho_{sl} = 0.934$, $\rho_{bl} = 0.934$, $\mu_{gl} = 0.001$, $\mu_{sl} = 1$, $\mu_{bl} = 1$, $k_{gl} = 0.04$, $k_{sl} = 3.8$, $k_{bl} = 3.8$, $C_{pgl} = 0.24$, $C_{psl} = 0.5$, $C_{pbl} = 0.5$, $\sigma_{ls,gl} = 0.356$, $\sigma_{lb,gl} = 0.412$, $\sigma_{sb,gl} = 0.356$ and $\sigma_{gb,gl} = 1$. Simulations are done for three values of $\sigma_{gs,gl} = 0.8$, 1 and 1.2. The results are shown for in Figure 6. Here we note that in the simulations the imposed Weber number is $We = 1.4e-7 \times 400$.

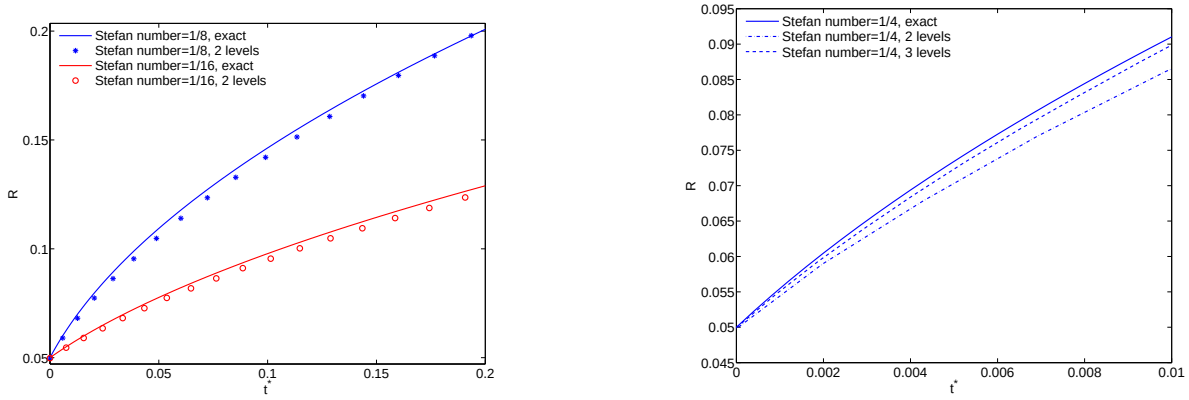


(a) Results for different Stefan numbers

(b) Convergence under grid refinement

**Figure 5. Simulated and exact position of the freezing front in time.**

Figure 6.a-c show the dependency of the triple point angles to changes in surface tension values. In this case, increase in the surface tension between air and ice leads to reduction of the water angle in the triple point junction. Also, numerical results show qualitative agreement with experimental results in the sense that we obtain similar conical freezing geometries after the water droplet has completely turned into ice (Figure 6.e).

## IV.C. Impact and solidification of a water droplet on a flat surface

In this test, we simulate the impact of a supercooled water droplet onto a flat surface made of ice. The computational domain is a RZ 3D axisymmetric grid with size $6 \times 12$ (dimensionless units). A $32 \times 64$ base grid with 2 levels of adaptivity is used. The base dimensionless parameters for this problem are: $St = 0.75$, $Pr = 14.4$, $Bo = 1.8e6$, $We = 1.4e-7$ $\rho_{gl} = 0.000623$, $\rho_{sl} = 0.934$, $\mu_{gl} = 0.005$, $\mu_{sl} = 1$, $k_{gl} = 0.04$, $k_{sl} = 3.8$, $C_{pgl} = 0.24$, $C_{psl} = 0.5$, $\sigma_{ls,gl} = 0.356$ and $\sigma_{gs,gl} = 0.95$.

The water droplet is initially a sphere with size $r = 0.153\,\text{cm}$. The distance between the center of droplet and the ice surface is 0.75 (dimensionless). Water is supercooled at $T_l = 268\,\text{K}$ and the base ice material is kept at $T_s = 258\,\text{K}$. A dimensionless impact velocity of 1545 is prescribed (see Figure 4.c for the initial and boundary conditions). Here we note that in the simulations the imposed Weber number and bond numbers are $We = 1.4e-7 \times 100$ and $Bo = 1.8e4 \times 100$.

### *IV.C.1. Stefan number*

First, we look at the sensitivity of the impact and freezing process to the Stefan number. Three values of 0.075, 0.75 and 7.5 are picked for the Stefan number. As shown by the results in Figure 7, a greater Stefan number leads to a faster freezing process. For the case $St = 0.075$, during the impact and initial spreading the amount of frozen water is negligible (Figure 7.a). After retraction (Figure 7.b), the freezing process slowly continues (Figure 7.c) resulting in a frozen droplet with the shape similar to the solidification of an initially static droplet. For the case $St = 0.75$, during the impact and spreading a very small amount of freezing is observed (Figure 7.d). While remaining water phase retracting, freezing continues (Figure 7.e). The freezing process is faster and by the time $t^* = 0.3$ the whole droplet is frozen. The different stages of spreading and retracting can be seen as the different cone slope on the final frozen droplet (Figure 7.f). For the case with the largest Stefan number $St = 7.5$, significant freezing is occurred during the impact and spreading (Figure 7.g). While the remaining water is retracting, freezing continues rapidly (Figure 7.h). Since the freezing process is much faster compared to previous cases, the whole droplet is frozen by the time $t^* = 0.0047$ and has a more spread-out shape (Figure 7.i).

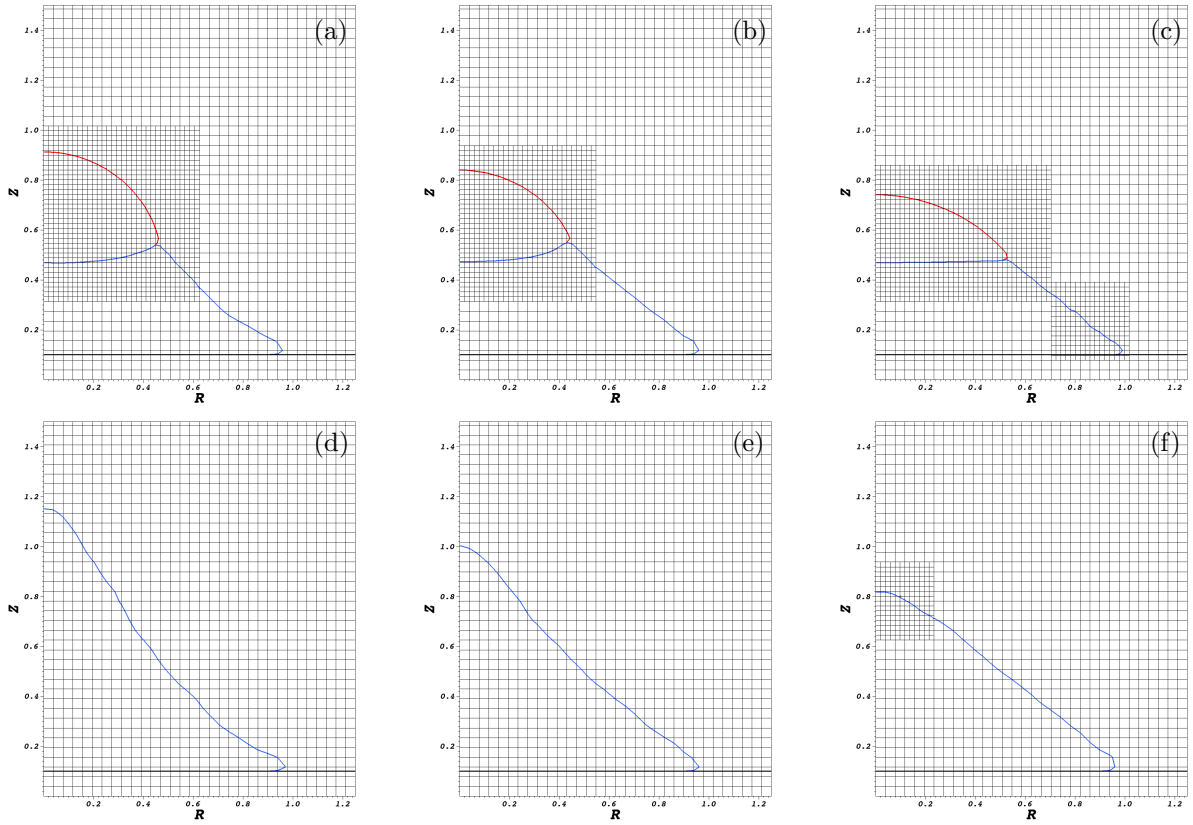


**Figure 6. Freezing of a water droplet on a flat surface. For reference, see experiments.[48] (a) $\sigma_{gs,gl} = 0.8$ and $t^* = 0.086$. (b) $\sigma_{gs,gl} = 1.0$ and $t^* = 0.086$. (c) $\sigma_{gs,gl} = 1.2$ and $t^* = 0.086$. (d) $\sigma_{gs,gl} = 0.8$ and $t^* = 0.30$. (e) $\sigma_{gs,gl} = 1.0$ and $t^* = 0.24$. (f) $\sigma_{gs,gl} = 1.2$ and $t^* = 0.29$. Top row simulations are at time $t^* = 0.086$, while the bottom row results are depicted when all water is turned to ice. Red lines show the boundary of liquid phase, blue lines show the boundary of ice phase and black lines show the substrate surface. Meshes show the grid levels used in the simulation.**

### *IV.C.2. Droplet size*

The size of the droplet has effects on the impact dynamics and freezing time. To demonstrate this effect we simulated the impact and freezing of droplets with half and twice the size of the base case that we discussed in the previous section. The dimensionless parameters are the same with the exception that $St = 0.375$ is used here. The droplets with different sizes $r_{c,1} = 0.0765\,\text{cm}$, $r_{c,2} = 0.153\,\text{cm}$ and $r_{c,3} = 0.306\,\text{cm}$ have different characteristic times $t_{c,1} = 4.22\,\text{s}$, $t_{c,2} = 16.89\,\text{s}$ and $t_{c,3} = 67.57\,\text{s}$. As the simulation result shows, at the same physical time $t = 0.45\,\text{s}$, the height of the frozen layers are similar. That is, the height of the frozen layer is independent of the droplet size. However, the larger the droplet, more ripples are observed during the spreading and retraction stages. This can create more roughly-shaped frozen layers specifically at the perimeter of the frozen droplet. Also the overall shape of the droplet and frozen part is similar at the same dimensionless time for different droplet sizes. This indicates that the characteristic time $t_c = \rho_l C_{pl} r_c^2 / k_l$ is an appropriate choice for the droplet freezing problem.

### *IV.C.3. Surface wettability*

The surface wettability property has significant effect on the behavior of the impacting droplet. Here we are looking at three distinct cases of hydrophilic, hydrophobic and super-hydrophobic surfaces. The setup and dimensionless parameters are the same as the base case discussed in IV.C.1, except the impact velocity, which is set to 15457.48 (dimensionless unit) to be comparable to the experiments of Mishchenko et al. [49] We change the surface tension between the liquid droplet and the ice flat base to emulate the different wettability

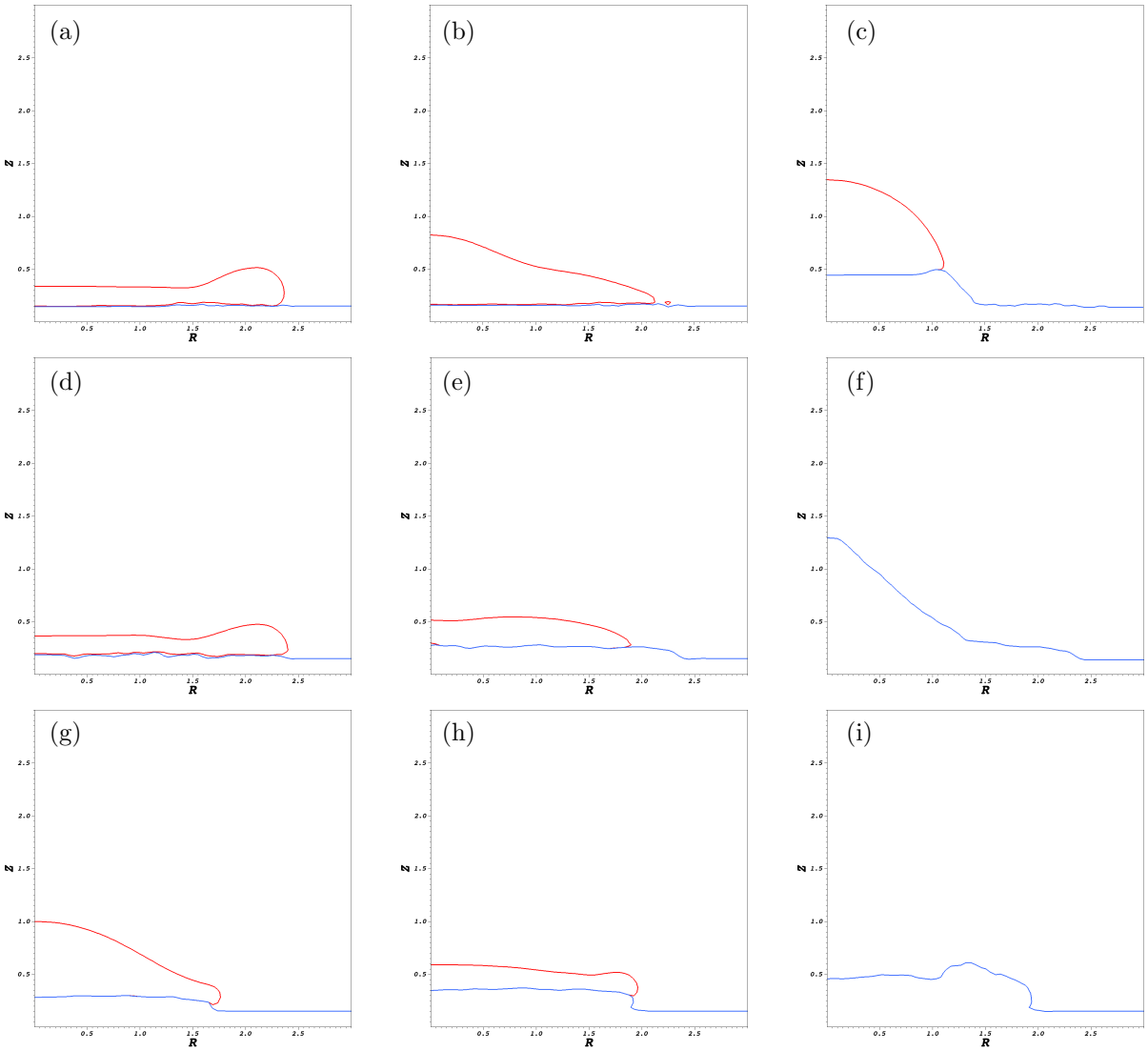


**Figure 7. Impact and freezing of a water droplet on a flat ice surface. (a)** $St = 0.075$ **and** $t^* = 0.0026$**. (b)** $St = 0.075$ **and** $t^* = 0.0076$**. (c)** $St = 0.075$ **and** $t^* = 0.3$**. (d)** $St = 0.75$ **and** $t^* = 0.0026$**. (e)** $St = 0.75$ **and** $t^* = 0.0076$**. (f)** $St = 0.75$ **and** $t^* = 0.3$**. (g)** $St = 7.5$ **and** $t^* = 0.001$**. (h)** $St = 7.5$ **and** $t^* = 0.0018$**. (i)** $St = 7.5$ **and** $t^* = 0.0047$**. Red lines show the water phase in droplets and blue lines show the ice phase.**

properties:

| | | |
|---|---|---|
| $\sigma_{ls,gl} = 0.068$ | $\theta = 21.4°$ | (hydrophilic) |
| $\sigma_{ls,gl} = 1.373$ | $\theta = 111.9°$ | (hydrophobic) |
| $\sigma_{ls,gl} = 1.991$ | $\theta = 172.6°$ | (super-hydrophobic) |

Here $\theta$ is the contact angle of the water on the surface at rest.

For the hydrophilic surface the droplet spreads out on the surface after the impact and freezes without any significant retraction (Figure 9). For the hydrophobic surface, the droplet spreads out on the surface (Figure 10.a) and retracts to reach a maximum height (Figure 10.b). It continues to freeze with a conical form (Figure 10.c). For the super-hydrophobic surface, the droplet spreads out on the surface upon impact (Figure 11.a) and retracts to reach a maximum height while in contact with the surface (Figure 11.b) and bounces back to leave the surface (Figure 11.c).

These test show the significance of the airplane surface wettability properties in avoiding the freezing problem instead of using thermal or pneumatic deicing techniques.[49,50]

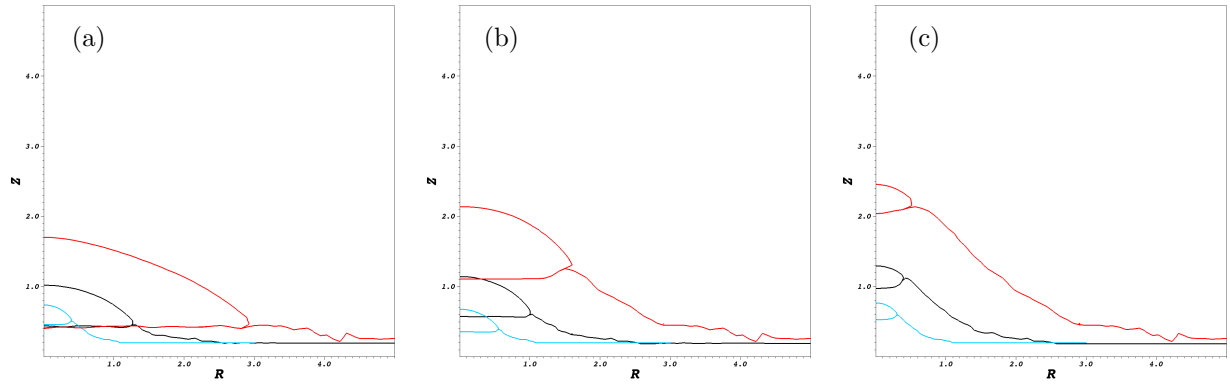


**Figure 8. Impact and freezing of water droplets with different sizes on a flat ice surface. (a)** $t = 0.45\,\mathrm{s}$ **(b)** $t_1^* = t_2^* = t_3^* = 0.1$ **(c)** $t_1^* = t_2^* = t_3^* = 0.28$**. Droplets with radius** $r_{c,1} = 0.0765\,\mathrm{cm}$**,** $r_{c,2} = 0.153\,\mathrm{cm}$ **and are shown with color blue, black and red respectively.**

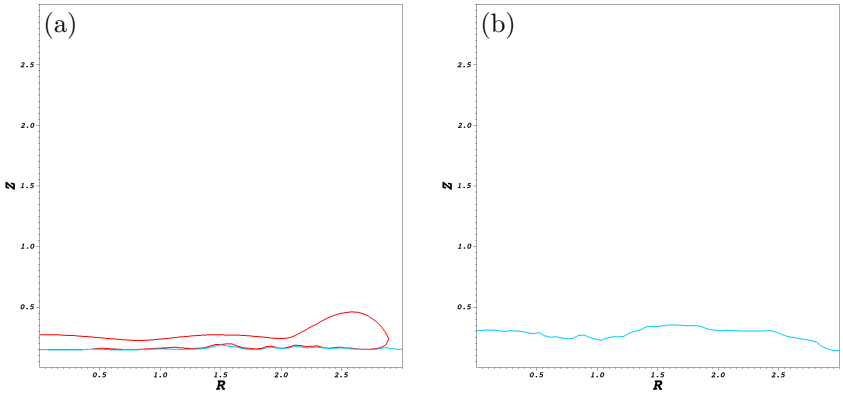


**Figure 9. Impact and freezing of a water droplet on a hydrophilic surface (a) Maximum spread at** $t^* = 0.00035$ **(b) Final freezing time** $t^* = 0.13$**.**

## V. Conclusions

We have developed a novel numerical method for simulating the impact and freezing of water droplets on surfaces. The moment-of-fluid representation lends itself to the simulation of multimaterial problems with triple junctions. We have attained quantitative agreement with the analytical solutions for an expanding circular ice patch, and qualitative agreement with experiments for the conversion of a water droplet on a substrate to ice,[48] and impact and solidification of a water droplet on a flat surface.[49] Parameter study for the impact and solidification of a single droplet showed that a larger Stefan number causes the shape of the resulting frozen droplet to deviate from the conical form and instead attain more unpredictable shapes. The change of the droplet size has a minimal effect on the shape of the frozen droplet at the impact point, and larger impacting droplets can create rough frozen layers in the perimeter regions. Surface wettability has substantial effect on the terminal behavior of the droplet. An impacting droplet will spread out and freeze on a hydrophilic surface and bounce back on a super-hydrophobic surface without icing taking place.

The developed numerical method has shown promising results studying the droplet impact and solidification process. We will use this method to do a comprehensive study of droplet impact and solidification at flight conditions taking into the account environmental parameters such as cross-flow air and various impact angles.

## References

[1]Bragg, M., "Aerodynamics of supercooled-large-droplet ice accretion and the effect on aircraft control," *Proceedings of the FAA International Conference on Aircraft Inflight Icing*, Vol. 2, 1996, pp. 387–399.

[2]Cebeci, T. and Kafyeke, F., "Aircraft icing," *Annual review of fluid mechanics*, Vol. 35, No. 1, 2003, pp. 11–21.

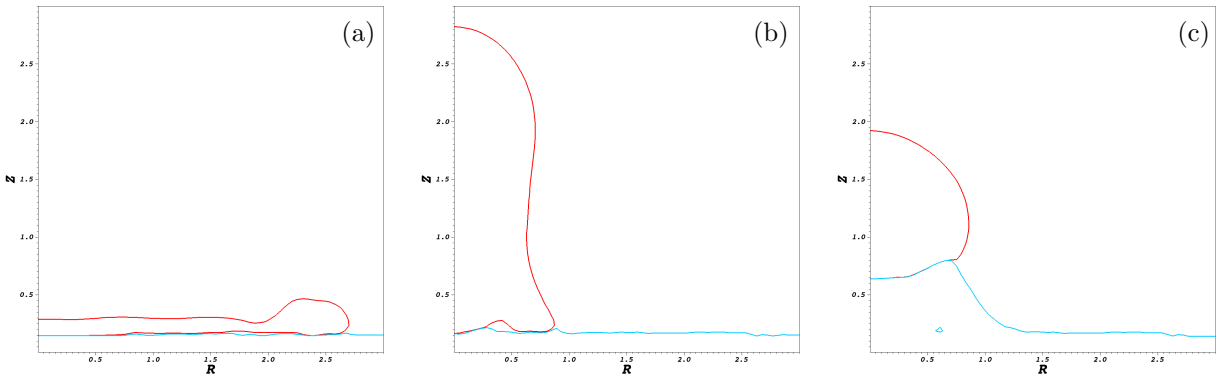


**Figure 10. Impact and freezing of a water droplet on a hydrophobic surface (a) Maximum spread at $t^* = 0.00027$ (b) Retraction to maximum height $t^* = 0.00185$. (c) freezing continues $t^* = 0.056$**

[3]Gent, R., Dart, N., and Cansdale, J., "Aircraft icing," *Philosophical Transactions of the Royal Society of London. Series A: Mathematical, Physical and Engineering Sciences*, Vol. 358, No. 1776, 2000, pp. 2873–2911.

[4]Lynch, F. T. and Khodadoust, A., "Effects of ice accretions on aircraft aerodynamics," *Progress in Aerospace Sciences*, Vol. 37, No. 8, 2001, pp. 669–767.

[5]Shin, J. and Bond, T. H., *Results of an icing test on a NACA 0012 airfoil in the NASA Lewis Icing Research Tunnel*, National Aeronautics and Space Administration, 1992.

[6]Addy Jr, H. E., "Ice accretions and icing effects for modern airfoils," Tech. rep., DTIC Document, 2000.

[7]Bragg, M., Broeren, A., Addy, H., Potapczuk, M., Guffond, D., and Montreuil, E., "Airfoil ice-accretion aerodynamics simulation," *AIAA Paper*, Vol. 85, 2007, pp. 22.

[8]Ruff, G. A. and Berkowitz, B. M., "Users manual for the NASA Lewis ice accretion prediction code (LEWICE)," 1990.

[9]Wright, W., "User's Manual for LEWICE Version 3.2," 2008.

[10]Tran, P., Brahimi, M., Paraschivoiu, I., Pueyo, A., and Tezok, F., "Ice accretion on aircraft wings with thermodynamic effects," *Journal of aircraft*, Vol. 32, No. 2, 1995, pp. 444–446.

[11]Saeed, F., "State-of-the-art aircraft icing and anti-icing simulation," *ARA (American Romanian Academy) Journal*, 2000, pp. 2000–2002.

[12]Nakakita, K., Nadarajah, S., and Habashi, W., "Toward real-time aero-icing simulation of complete aircraft via FENSAP-ICE," *Journal of Aircraft*, Vol. 47, No. 1, 2010, pp. 96–109.

[13]Rein, M., "Phenomena of liquid drop impact on solid and liquid surfaces," *Fluid Dynamics Research*, Vol. 12, No. 2, 1993, pp. 61.

[14]Politovich, M. K., "Aircraft icing caused by large supercooled droplets," *Journal of Applied Meteorology*, Vol. 28, No. 9, 1989, pp. 856–868.

[15]Marwitz, J., Politovich, M., Bernstein, B., Ralph, F., Neiman, P., Ashenden, R., and Bresch, J., "Meteorological conditions associated with the ATR72 aircraft accident near Roselawn, Indiana, on 31 October 1994," *Bulletin of the American Meteorological Society*, Vol. 78, No. 1, 1997, pp. 41–52.

[16]Potapczuk, M. G., "Semi-empirical modeling of SLD physics," 2004.

[17]Broeren, A. P., Whalen, E. A., Busch, G. T., and Bragg, M. B., "Aerodynamic simulation of runback ice accretion," *Journal of Aircraft*, Vol. 47, No. 3, 2010, pp. 924–939.

[18]Zhang, K., Blake, J., and Rothmayer Alric, H. H., "An Experimental Investigation on Wind-Driven Rivulet/Film Flows over a NACA0012 Airfoil by Using Digital Image Projection Technique," 2014.

[19]Latka, A., Strandburg-Peshkin, A., Driscoll, M. M., Stevens, C. S., and Nagel, S. R., "Creation of prompt and thin-sheet splashing by varying surface roughness or increasing air pressure," *Physical review letters*, Vol. 109, No. 5, 2012, pp. 054501.

[20]Xu, L., Zhang, W. W., and Nagel, S. R., "Drop splashing on a dry smooth surface," *Physical review letters*, Vol. 94, No. 18, 2005, pp. 184505.

[21]Madejski, J., "Solidification of droplets on a cold surface," *International Journal of Heat and Mass Transfer*, Vol. 19, No. 9, 1976, pp. 1009–1013.

[22]Schiaffino, S. and Sonin, A. A., "Molten droplet deposition and solidification at low Weber numbers," *Physics of Fluids (1994-present)*, Vol. 9, No. 11, 1997, pp. 3172–3187.

[23]Davis, S. H., *Theory of solidification*, Cambridge University Press, 2001.

[24]Pasandideh-Fard, M., Bhola, R., Chandra, S., and Mostaghimi, J., "Deposition of tin droplets on a steel plate: simulations and experiments," *International Journal of Heat and Mass Transfer*, Vol. 41, No. 19, 1998, pp. 2929–2945.

[25]Pasandideh-Fard, M., Chandra, S., and Mostaghimi, J., "A three-dimensional model of droplet impact and solidification," *International Journal of Heat and Mass Transfer*, Vol. 45, No. 11, 2002, pp. 2229–2242.

[26]Le Bot, C., Vincent, S., and Arquis, E., "Impact and solidification of indium droplets on a cold substrate," *International Journal of Thermal Sciences*, Vol. 44, No. 3, 2005, pp. 219–233.

[27]Xu, J., Smith, K., Celik, D., Hussaini, M., and Van Sciver, S., "Hydrogen particles in liquid helium," *Cryogenics*, Vol. 44, No. 6, 2004, pp. 507–514.

[28]Unlusu, B., Xu, J., Hussaini, M. Y., Celik, D., and Van Sciver, S. W., "Investigation of Hydrogen Droplet Solidification in Cryogenic Helium," *Journal of Thermophysics and Heat Transfer*, Vol. 22, No. 1, 2008, pp. 83–89.

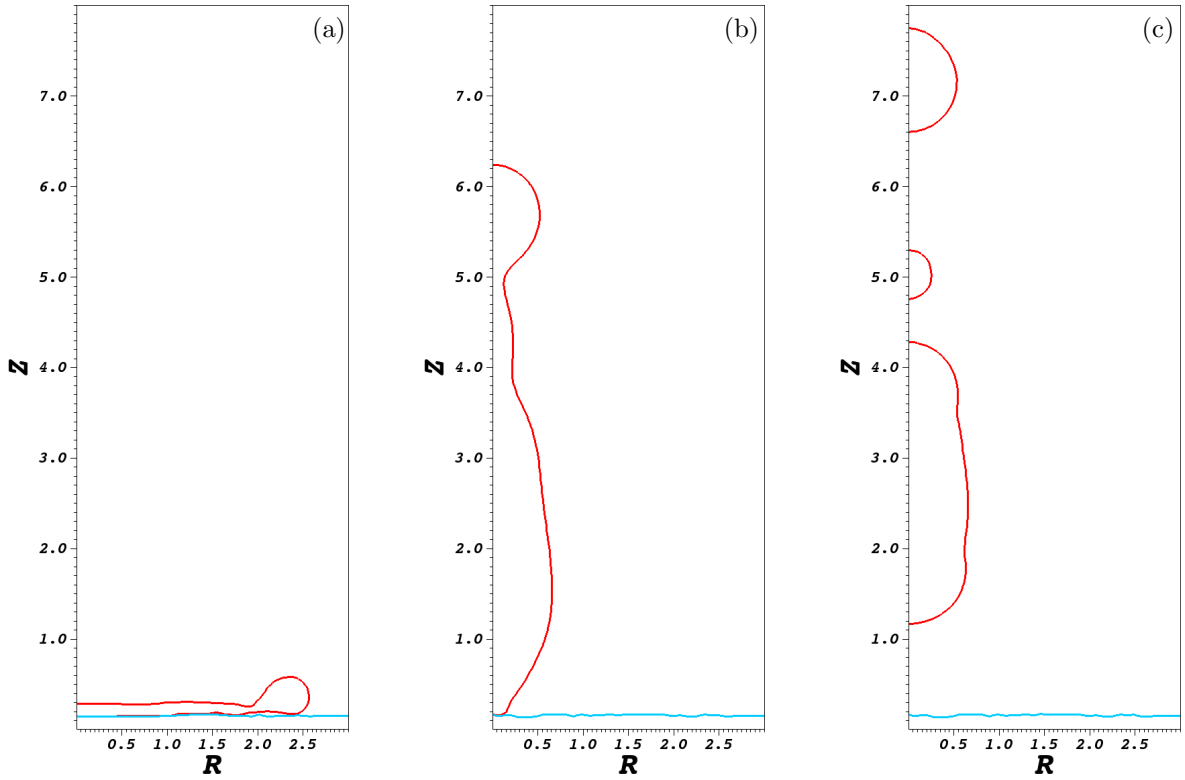


**Figure 11. Impact and freezing of a water droplet on a super-hydrophobic surface (a) Maximum spread at $t^* = 0.00027$ (b) Retraction to maximum height while in contact with surface $t^* = 0.0011$. (c) bouncing back $t^* = 0.0013$**


[29]Zheng, L. and Zhang, H., "An adaptive level set method for moving-boundary problems: application to droplet spreading and solidification," *Numerical Heat Transfer: Part B: Fundamentals*, Vol. 37, No. 4, 2000, pp. 437–454.

[30]Mihalef, V., Unlusu, B., Metaxas, D., Sussman, M., and Hussaini, M. Y., "Physics based boiling simulation," *Proceedings of the 2006 ACM SIGGRAPH/Eurographics symposium on Computer animation*, Eurographics Association, 2006, pp. 317–324.

[31]Gibou, F., Chen, L., Nguyen, D., and Banerjee, S., "A level set based sharp interface method for the multiphase incompressible Navier–Stokes equations with phase change," *Journal of Computational Physics*, Vol. 222, No. 2, 2007, pp. 536–555.

[32]Esmaeeli, A. and Tryggvason, G., "Computations of film boiling. Part I: numerical method," *International Journal of Heat and Mass Transfer*, Vol. 47, No. 25, 2004, pp. 5451–5461.

[33]Esmaeeli, A. and Tryggvason, G., "Computations of film boiling. Part II: multi-mode film boiling," *International journal of heat and mass transfer*, Vol. 47, No. 25, 2004, pp. 5463–5476.

[34]Vu, T. V., Tryggvason, G., Homma, S., Wells, J. C., and Takakura, H., "A Front-Tracking Method for Three-Phase Computations of Solidification with Volume Change," *Journal of Chemical Engineering of Japan*, Vol. 46, No. 11, 2013, pp. 726–731.

[35]Dyadechko, V. and Shashkov, M., "Moment-of-fluid interface reconstruction," *Los Alamos report LA-UR-05-7571*, 2005.

[36]Ahn, H. T. and Shashkov, M., "Multi-material interface reconstruction on generalized polyhedral meshes," *Journal of Computational Physics*, Vol. 226, No. 2, 2007, pp. 2096–2132.

[37]Dyadechko, V. and Shashkov, M., "Reconstruction of multi-material interfaces from moment data," *Journal of Computational Physics*, Vol. 227, No. 11, 2008, pp. 5361–5384.

[38]Ahn, H. T. and Shashkov, M., "Adaptive moment-of-fluid method," *Journal of Computational Physics*, Vol. 228, No. 8, 2009, pp. 2792–2821.

[39]Ahn, H. T., Shashkov, M., and Christon, M. A., "The moment-of-fluid method in action," *communications in Numerical Methods in Engineering*, Vol. 25, No. 10, 2009, pp. 1009–1018.

[40]Jemison, M., Sussman, M., and Arienti, M., "Compressible, multiphase semi-implicit method with moment of fluid interface representation," *Journal of Computational Physics*, Vol. 279, 2014, pp. 182–217.

[41]Jemison, M., Loch, E., Sussman, M., Shashkov, M., Arienti, M., Ohta, M., and Wang, Y., "A coupled level set-moment of fluid method for incompressible two-phase flows," *Journal of Scientific Computing*, Vol. 54, No. 2-3, 2013, pp. 454–491.

[42]Lian, Y. and Guo, Y., "Investigation of the Splashing Phenomenon of Large Droplets for Aviation Safety," Tech. rep., SAE Technical Paper, 2015.

[43]Son, G. and Hur, N., "A coupled level set and volume-of-fluid method for the buoyancy-driven motion of fluid particles," *Numerical Heat Transfer: Part B: Fundamentals*, Vol. 42, No. 6, 2002, pp. 523–542.

[44]Bonhomme, R., Magnaudet, J., Duval, F., and Piar, B., "Inertial dynamics of air bubbles crossing a horizontal fluid–fluid interface," *Journal of Fluid Mechanics*, Vol. 707, 2012, pp. 405–443.

[45]Li, G., Lian, Y., Guo, Y., Jemison, M., Sussman, M., Helms, T., and Arienti, M., "Incompressible Multiphase flow and Encapsulation simulations using the moment of fluid method," 2015, Accepted in International Journal for Numerical Methods in Fluids.

[46]Gibou, F., Fedkiw, R. P., Cheng, L.-T., and Kang, M., "A second-order-accurate symmetric discretization of the Poisson equation on irregular domains," *Journal of Computational Physics*, Vol. 176, No. 1, 2002, pp. 205–227.

[47]Carslaw, H. S., Jaeger, J. C., et al., *Conduction of heat in solids*, Vol. 2, Clarendon Press Oxford, 1959.

[48]Enri´ quez, O. R., Mari´ n, A. l. G., Winkels, K. G., and Snoeijer, J. H., "Freezing singularities in water drops," *Physics of fluids*, Vol. 24, No. 9, 2012, pp. 091102.

[49]Mishchenko, L., Hatton, B., Bahadur, V., Taylor, J. A., Krupenkin, T., and Aizenberg, J., "Design of ice-free nanostructured surfaces based on repulsion of impacting water droplets," *ACS nano*, Vol. 4, No. 12, 2010, pp. 7699–7707.

[50]Jung, S., Dorrestijn, M., Raps, D., Das, A., Megaridis, C. M., and Poulikakos, D., "Are superhydrophobic surfaces best for icephobicity?" *Langmuir*, Vol. 27, No. 6, 2011, pp. 3059–3066.